NOMA-Aided Multi-UAV Communications in Full-Duplex Heterogeneous Networks

Tan Zheng Hui Ernest, A S Madhukumar, Rajendra Prasad Sirigina, and Anoop Kumar Krishna

***Abstract*—To address spectrum scarcity in unmanned aerial vehicle (UAV) communications, non-orthogonal multiple access (NOMA) aided multi-UAV communications in full-duplex (FD) heterogeneous networks (HetNets) is investigated in this paper. Specifically, an ergodic capacity analysis of NOMA-aided multi-UAV communications in FD-HetNets is conducted through a moment generating function (MGF) approach within a stochastic geometry framework. By employing the MGF approach to evaluate ergodic capacity, exact expressions that are simpler to evaluate are obtained. When compared against half-duplex HetNets, i.e., HD-HetNets, FD-HetNets with effective interference management enable higher ergodic capacity to be obtained by the macro base station and UAVs. Furthermore, we show that it is possible for NOMA-aided multi-UAV communications in FD-HetNets to achieve higher ergodic sum capacity and ergodic capacity gains than HD-HetNets while supporting more UAVs at low altitude due to a stronger desired signal. Even with lower levels of self-interference (SI) suppression and strong phase noise, NOMA-aided multi-UAV communications in FD-HetNets is still able to achieve higher ergodic sum capacity over HD-HetNets. Therefore, the attractiveness of NOMA-aided multi-UAV communications in FD-HetNets is highlighted as a promising solution towards improving spectrum utilization in UAV communications.**

***Index Terms*—Unmanned Aerial Vehicle, Full-Duplex, Ergodic Capacity, Rician Fading, Stochastic Geometry, Heterogeneous Networks.**

I. Introduction

Unmanned aerial vehicles (UAVs) are expected to play an important role in future wireless networks, with diverse use cases being proposed in both industry and academia. Applications involving multi-UAV networks have, for instance, been envisaged to provide temporary wireless services in disaster-struck areas [1]. Other prominent concepts that have attracted recent research attention include the deployment of UAVs as aerial base stations (BSs) [2]–[4], relays [5], or user equipments (UEs) [6]–[9].

Yet, the planned ubiquity of UAVs in future wireless networks ultimately places a strain on the availability of spectrum to support UAV communications. Just as spectrum scarcity is an issue in many other systems, e.g., cellular communications [5], [10], spectrum scarcity is also an issue in unmanned aerial vehicle (UAV) communications as the allocated L-band and C-band are also shared with other existing systems [11], [12]. Therefore, only a limited part of the allocated bands can be used to support UAV communications, resulting in a constraint on the number of deployed UAVs in a network [11], [12]. Furthermore, a shortage of available spectrum may lead to a performance degradation of multi-UAV networks [13].

In this regard, non-orthogonal multiple access (NOMA), i.e., power-domain NOMA, has been investigated in the literature to improve spectrum efficiency. The concept of NOMA hinges on the fact that nodes in NOMA-aided systems are multiplexed in the power-domain to share the same spectrum. In contrast, conventional orthogonal multiple access schemes employ orthogonal allocation of time-frequency resource blocks for each node in the network. Thus, compared to orthogonal multiple access systems, NOMA-aided systems are capable of achieving higher spectrum utilization. When adopted for multi-UAV communications, superposition coding is employed to enforce unequal power allocation for all UAVs and ground stations (GSs). Thereafter, the desired messages are recovered at the receivers via successive interference cancellation (SIC) when the interference is stronger than the desired message [14]–[20]. For receivers experiencing weak interference, the desired message is simply detected by treating interference as noise [14], [20].

Already, NOMA has been investigated as a means to improve spectrum efficiency in heterogeneous networks (HetNets) for cellular communications [21], [22] and UAV communications [23]. Although promising, the orthogonal allocation of time-frequency resources is still necessary as power-domain multiplexing is only employed during uplink (UL) or downlink (DL) transmissions [8], [24].

To further address spectrum scarcity, one can consider integrating NOMA-aided multi-UAV communications into full-duplex (FD) HetNets, i.e., FD-HetNets, comprising FD-capable GSs (FD-GSs) and half-duplex (HD) macro base stations (MBSs). In particular, implementing NOMA-aided multi-UAV communications in FD-HetNets enable UL UAVs and DL UAVs, equipped with conventional HD transceivers, to simultaneously operate on the same spectrum thanks to the operation of FD-GSs. As compared to conventional NOMA-aided half-duplex HetNets (HD-HetNets), where all nodes operate in HD mode, higher spectrum efficiency can be attained via NOMA-aided FD-HetNets. However, such FD-based systems are also impaired by residual self-interference (SI) due to carrier phase noise and imperfect SI channel estimation [25], and interference from UL UAVs [7]–[9].

Tan Zheng Hui Ernest is with the School of Computer Science and Engineering, Nanyang Technological University, Singapore e-mail: (tanz0119@e.ntu.edu.sg).

A S Madhukumar is with the School of Computer Science and Engineering, Nanyang Technological University, Singapore e-mail: (asmadhukumar@ntu.edu.sg).

Rajendra Prasad Sirigina is with the School of Computer Science and Engineering, Nanyang Technological University, Singapore e-mail: (raje0015@e.ntu.edu.sg).

Anoop Kumar Krishna is with Airbus Singapore Pte Ltd, Singapore e-mail: (anoopkumar.krishna@airbus.com).

A. Related Literature

Despite being limited by residual SI and UL interference, NOMA-aided FD-HetNets have started receiving interest in the literature as a potential solution to address spectrum scarcity. For instance, a power control technique was proposed in [26] for interference management in a NOMA-aided FD-HetNet, with similar works on NOMA-aided HD-HetNets [21], [22] also noted.

For UAV communications in FD-HetNets and HD-HetNets, there exists limited studies in the literature. For instance, the work in [23] analyzed the optimization of resource allocation in HD-HetNets. Likewise, the authors in [27] studied UAV placement to optimize network delays. For UAV communications in FD-HetNets, throughput optimization through UAV placement and resource allocation was investigated in [28] and [29]. While some of the above studies have looked at throughput as a key metric, an accurate characterization of the ergodic capacity for FD-HetNets in multi-UAV communications is currently lacking.

Although there exists some works on NOMA-aided FD-HetNets and NOMA-aided HD-HetNets in cellular networks, the obtained conclusions may not be readily applied for multi-UAV communications due to differences in operating environments and deployment constraints between cellular and multi-UAV systems.

One such difference is the channel model for both cellular and UAV communications. In cellular communications, Rayleigh fading [24] and Nakagami-*m* fading [10], [30] are commonly assumed. However, apart from UAV communications taking place over Rayleigh fading [31], [32] and Nakagami-*m* fading [6], other types of fading can also be encountered. For instance, transmissions over Rician fading channels have been noted for UAV-to-GS links [7]–[9], [33], [34] and UAV-to-UAV links [7], [9], [35]. Channel measurement campaigns in [11], [12], [36] have also confirmed the suitability of modeling UAV links as Rician fading channels.

Another difference stems from the spatial distribution of nodes in cellular and UAV communications. As discussed earlier, the application of UAVs in future wireless networks has garnered intense interest in deploying UAV-aided wireless connectivity via aerial BSs or relays. However, one will need to account for the spatial location and mobility of the UAVs before any accurate performance evaluation is possible. To help accomplish such a feat, one can employ the useful tools of stochastic geometry for multi-UAV networks. A common technique seen in the literature involves modeling the spatial location of UEs as a Poisson point process (PPP).

While PPPs have been extensively used to analyze cellular networks, a PPP effectively covers an infinite region [6]. Furthermore, the number of nodes modeled at each instance of a PPP is not fixed. In contrast, UAV networks are more likely to be deployed over a small region with fixed numbers of deployed UAVs [3], [6].

In light of the above discussions, the homogeneous binomial point process (BPP) model is more suitable in modeling the spatial locations of UAVs [3], [6]. Compared to PPPs, the BPP model allows for the area of the considered region, i.e., area of the cell, to be defined. Also, in contrast to PPPs, BPPs enable the number of deployed nodes, i.e., UAVs, at every realization to be fixed, while ensuring that the spatial locations of the nodes are uniformly distributed.

B. Motivation and Main Contributions

In spite of several studies that have analyzed multi-UAV networks using the BPP model, e.g., [3], [4], [6], similar studies involving NOMA-aided multi-UAV communications in FD-HetNets are lacking in the literature. Specifically, the performance of multi-UAV deployments in NOMA-aided FD-HetNets is currently unclear. Key design parameters and insights concerning NOMA-aided multi-UAV communications in the FD-HetNet over Rician fading channels in the presence of interference are unknown. Examples of key design parameters and insights include the number of deployed UAVs, impact of UAV altitude, throughput of UAV communications in NOMA-aided FD-HetNets, and the impact of SI and residual interference on the NOMA-aided FD-HetNets.

Based on the above discussions, an ergodic capacity analysis of NOMA-aided multi-UAV communications in a FD-HetNet is conducted in this paper. By considering Rician fading channels and the BPP model for UAV spatial location modeling, a realistic performance analysis framework is proposed where we demonstrate the feasibility and advantages of NOMA-aided multi-UAV communications in FD-HetNets. As compared to similar works done in the context of cellular networks, e.g., [21] and [22], the focus of the present work is different, since key design parameters and insights are yielded based on the ergodic capacity performance of NOMA-aided multi-UAV FD-HetNets. To the best of the authors knowledge, such analysis in the context of NOMA-aided multi-UAV networks are currently not available in the literature.

The major contributions of this paper are thus summarized as follows:

- This paper presents exact ergodic capacity expressions over Rician fading channels for NOMA-aided multi-UAV communications in FD-HetNets and HD-HetNets under a BPP-based stochastic geometry framework.
- The benefits of NOMA-aided multi-UAV communications in FD-HetNets over HD-HetNets are demonstrated. Specifically, NOMA-aided multi-UAV FD-HetNets achieve higher ergodic capacity at the node and system level while enabling more UAVs to be deployed over HD-HetNets.
- Exact ergodic capacity gains of FD-HetNets over HD-HetNets for NOMA-aided multi-UAV are also presented, where the feasibility of NOMA-aided multi-UAV FD-HetNets through effective interference management is highlighted.

The remainder of this paper is organized as follows. The system model is introduced in Section II, with ergodic capacity expressions presented in Section III. Thereafter, numerical results are discussed in Section IV before the conclusion of the paper in Section V.

II. System Model

Consider a FD-HetNet supporting NOMA-aided multi-UAV communications in a suburban environment (Fig. 1). The

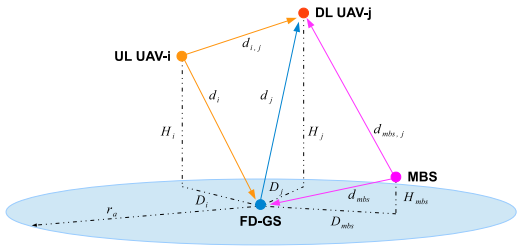

Fig. 1. The FD-HetNet for NOMA-aided multi-UAV communications is illustrated here. The FD-GS in the FD-HetNet enables HD uplink and downlink UAVs and the HD MBS to concurrently share the same spectrum for NOMA transmissions. Through the BPP, it is assumed that the spatial locations of the deployed UAVs and the MBS follow a uniform distribution around a disc, with origin O at the FD-GS and radius r_a.

FD-HetNet comprises N_U HD single-antenna UL UAVs, N_D HD single-antenna DL UAVs, one HD single-antenna MBS, and a FD-GS. In the rest of this section, the system model assumptions are first introduced. Then, the statistical distributions of the UAV and MBS spatial locations are discussed. Thereafter, the instantaneous signal-to-interference-plus-noise ratio (SINR) model for the FD-GS and downlink UAVs are presented.

A. System Model Assumptions

The FD-GS is assumed to be operating with one antenna each for signal transmission and reception, while the UL and DL UAVs function as aerial user equipments. It is also assumed that the FD-GS receives uplink data from the N_U UL UAVs and MBS-to-GS data from the MBS while concurrently transmitting DL data to the N_D DL UAVs on the same spectrum through power-domain NOMA. [1] Due to FD transmissions at the GS, the DL UAVs experience interference from the MBS and UL UAVs [7], [37], as well as multi-user interference (MUI) from other DL UAVs [8]. In this regard, the DL UAVs are assumed to be equipped with imperfect SIC detectors. For the FD-GS, SI mitigation is assumed and only residual SI is considered to account for FD transceiver impairments [7], [25], [37], [38]. Finally, it is assumed that the suburban UAV channel undergoes Rician fading [11], with compensated Doppler shift assumed in this paper [7], [37]. Rician fading is also assumed for the SI channel at the FD-GS to account for SI mitigation [7], [37], [38]. A summary of important notations is given in Table I.

B. Distance Distribution of the UAVs and MBS

Inspired by the studies in [3], [6], [38], the spatial locations of the UL UAVs, DL UAVs and the MBS are assumed to follow a BPP. Let the UL UAVs and DL UAVs be indexed by $1 \le i \le N_U$ and $1 \le j \le N_D$, respectively. Then, we denote $H_i = H_{min} + \omega\frac{i}{N_U}$ and $H_j = H_{min} + \omega\left[1 + \frac{i}{N_D}\right]$ as the respective altitudes (km) of UL UAV-i and DL UAV-j, where $\omega > 0$ indicates the altitude separation factor between the UL and DL UAVs, H_{min} denotes a minimum altitude such that $0 < H_{mbs} < H_{min}$, and H_{mbs} is the height of the MBS antenna.

[1] It is worth noting that such a system model has been studied in [28] and [29] in the context of aerial BSs.

TABLE I
SUMMARY OF IMPORTANT NOTATIONS

Notations	Description
$1 \le i \le N_U$	Index of UL UAV-i
$1 \le j \le N_D$	Index of DL UAV-j
H_{min}; ω	Minimum UAV altitude; Altitude separation factor
H_i; H_j	Altitude of UL UAV-i; Altitude of DL UAV-j
H_{mbs}	MBS antenna height
$H_{i,j}$	Altitude between UL UAV-i and DL UAV-j
$H_{mbs,j}$	Altitude between the MBS and DL UAV-j
d_{mbs}	Euclidean distance between the FD-GS and the MBS
d_i	Euclidean distance between the FD-GS and UL UAV-i
d_j	Euclidean distance between the FD-GS and DL UAV-j
$d_{mbs,j}$	Euclidean distance between the MBS and DL UAV-j
$d_{i,j}$	Euclidean distance between UL UAV-i and DL UAV-j
P_t; ρ	Transmit power; Normalized transmit power
P_{si}; ρ_{si}	Received power of the SI; Normalized SI power
σ^2	Strength of AWGN
ϵ	SI channel estimation error at the FD-GS
γ_ϕ^2	Strength of phase noise at the FD-GS oscillator
$\beta_{mbs,j}$	Residual interference from the MBS at DL UAV-j
$\beta_{i,j}$	Residual interference from UL UAV-i at DL UAV-j
α_j	NOMA power allocation factor for DL UAV-j

Based on the BPP assumption, let the spatial location of the UL UAVs, DL UAVs, and MBS be uniformly distributed around a disc with origin O at the FD-GS, radius r_a, and angle $[0, 2\pi)$ [6], [38]. The Euclidean distances (km) from the FD-GS to the MBS, UL UAV-i, and DL UAV-j are denoted as d_{mbs}, d_i, and d_j, respectively. For $x \in \{i, j, mbs\}$, the Euclidean distance d_x is defined as $d_x = \sqrt{D_x^2 + H_x^2}$, where D_x is the Euclidean distance between the projection of node-x onto the ground plane and the FD-GS. Finally, the inter-UAV distance between UL UAV-i and DL UAV-j is defined as $d_{i,j}$ while the distance between the MBS and DL UAV-j is denoted as $d_{mbs,j}$.

The probability density function (PDF) of d_x is given as $f_{d_x}(w_x) = \frac{2w_x}{r_a^2}$ [6, eq. (3)], where $x \in \{i, j, mbs\}$, $L_{m,x} \le w_x \le L_{p,x}$, $L_{m,x} = H_x$, and $L_{p,x} = \sqrt{H_x + r_a^2}$.

For the inter-UAV distance ($d_{i,j}$) and the distance between the MBS and DL UAV-j ($d_{mbs,j}$), the conditional PDF $f_{d_{x,j}}(w|d_j), x \in \{i, mbs\}$ is defined as [6, eq. (2)], [38, eq. (1)]:

$$f_{d_{x,j}}(w|d_j)=\begin{cases}\frac{2w}{r_a^2}, & H_{x,j} \le w \le L_{q,x}\\ \frac{2w}{\pi r_a^2}\arccos\left(\frac{w^2+d_j^2-\left(r_a^2+H_{x,j}^2\right)}{2d_j\sqrt{w^2-H_{x,j}^2}}\right), & L_{q,x} < w \le L_{r,x}\end{cases} \quad (1)$$

where $L_{q,x} = \sqrt{\left(r_a - d_j\right)^2 + H_{x,j}^2}$, $L_{r,x} = \sqrt{\left(r_a + d_j\right)^2 + H_{x,j}^2}$, $H_{i,j} = H_j - H_i$ is the separation altitude between UL UAV-i and DL UAV-j, and $H_{mbs,j} = H_j - H_{mbs}$ is the altitude between the MBS and DL UAV-j.

Through the PDFs, $f_{d_x}(w)$ and $f_{d_{x,j}}(w|d_j)$, a performance analysis of NOMA-aided multi-UAV communications in the FD-HetNet can be obtained with the spatial locations of the UAVs and MBS taken into consideration.

C. Instantaneous SINR at the FD-GS

To detect the messages transmitted by both the MBS and UL UAVs at the FD-GS, an SIC detection process is employed. [2] In particular, the FD-GS performs SIC to detect and remove the MBS signal of interest (SOI) from the received composite signal. The FD-GS then detects the SOI from the UL UAVs, starting with UL UAV-1, in the presence of MUI [16]–[20]. The SIC detection process is repeated until the SOIs of all the remaining UL UAVs are detected.

Let X_{mbs}, X_i, and $Y_{si,1}$ be non-centered Chi-squared distributed random variables (RVs) with respective Rician K factors K_{mbs}, K_i, and $K_{si,1}$. Also, let $Y_{si,2}$ be an exponentially distributed RV. Then, the instantaneous SINR to detect the SOI of the MBS at the FD-GS $\left(SINR_{mbs}^{FD}\right)$ is:

$$SINR_{mbs}^{FD} = \frac{\rho d_{mbs}^{-n} X_{mbs}}{1 + \rho \sum_{i=1}^{N_U} d_i^{-n} X_i + \rho_{si} Y_{si,1} + \rho_{si} Y_{si,2}}, \tag{2}$$

where n is the pathloss exponent, $\rho \propto \frac{P_t}{G\sigma^2}$ is the normalized transmit power [37], P_t is the transmit power, $G = \left(\frac{4\pi \cdot 10^9}{3 \cdot 10^8} f_c\right)^2$, f_c is the carrier frequency (MHz), $\sigma^2 = -174 + 10\log_{10}(B_W)$ is the strength of the additive white Gaussian noise (AWGN) in dBm [39], B_W is the bandwidth (Hz), $\rho_{si} = P_{si}/\sigma^2$ is the normalized power of the SI, $P_{si} = P_t$ denotes the received power of the SI, $X_{mbs} = |h_{mbs}|^2$, $X_i = |h_i|^2$, h_{mbs} is the channel between the FD-GS and the MBS, and h_i is the channel between the FD-GS and UL UAV-i. Also, $Y_{si,1} = \epsilon|\widetilde{h}_{si}|^2$ and $Y_{si,2} = \gamma_\phi^2 |h_{si}|^2$, where $\widetilde{h}_{si} = h_{si} - \widehat{h}_{si}$ is the error of the imperfect SI channel gain estimate, $\widehat{h}_{si}$ is the imperfect estimation of the SI channel gain, and γ_ϕ^2 is the strength of the Gaussian distributed phase noise [25]. [3] The SI channel estimation error $(\widetilde{h}_{si})$ is modeled as a circularly symmetric zero-mean complex Gaussian RV with variance ϵ to account for the worst case residual SI, [7], [37], [40]. In this way, the total amount of SI suppression to bring the residual SI signal below the noise floor (σ^2) is calculated as $1/(\epsilon\sigma^2)$ [37].

Similarly, the instantaneous SINR to detect the SOI of the UL UAVs at the FD-GS $\left(SINR_i^{FD}\right)$ is:

$$SINR_i^{FD} = \frac{\rho d_i^{-n} X_i}{1 + \sum_{k=i+1}^{N_U} \rho d_k^{-n} Y_k + \rho_{si} Y_{si,1} + \rho_{si} Y_{si,2}}, \tag{3}$$

where $Y_k = |h_k|^2$ is a non-centered Chi-squared distributed RV with Rician K factor K_k, and h_k is the channel between the FD-GS and the remaining UL UAVs.

D. Instantaneous SINR at Downlink UAV-j

At DL UAV-j, an SIC detector is employed to detect the SOI transmitted by the FD-GS. [4] In particular, the SIC detector at DL UAV-j detects the SOI in the presence of MUI from the other DL UAVs, as well as interference from both the UL UAVs and MBS.

Let X_j, $Y_{mbs,j}$, and $Y_{i,j}$ be non-centered Chi-squared distributed random variables (RVs) with respective Rician K factors K_i, $K_{mbs,j}$, and $K_{i,j}$. Then, the instantaneous SINR $\left(SINR_j^{FD}\right)$ at DL UAV-j is:

$$SINR_j^{FD} = \frac{\rho \alpha_j d_j^{-n} X_j}{1 + \rho d_{mbs,j}^{-n} Y_{mbs,j} + \rho d_j^{-n} X_j \sum_{k=1}^{j-1} \alpha_k + \rho \sum_{i=1}^{N_U} d_{i,j}^{-n} Y_{i,j}}, \tag{4}$$

where $X_j = |h_j|^2$, $Y_{mbs,j} = \beta_{mbs,j}|h_{mbs,j}|^2$, $Y_{i,j} = \beta_{i,j}|h_{i,j}|^2$, h_j is the channel between the FD-GS and DL UAV-j, $h_{mbs,j}$ is the channel between the MBS and DL UAV-j, $h_{i,j}$ is the channel between UL UAV-i and DL UAV-j, and α_j is the power allocation factor for DL UAV-j such that $\sum_{j=1}^{N_D} \alpha_j = 1$. Also, $0 \le \beta_{x,j} \le 1, x \in \{mbs, i\}$ is the strength of the residual interference after SIC [17], [41]–[43].

As the DL UAVs are deployed at different altitudes, i.e., $H_j < H_{j+1}$, the power allocation factor α_j can be heuristically defined based on the altitudes of the N_D DL UAVs to ensure fairness. In particular, the power allocation factor α_j can be defined as $\alpha_j = \frac{H_j}{\sum_{k=1}^{N_U} H_k}$, so that DL UAVs that are further away from the FD-GS are assigned higher transmit powers [22], i.e., $\alpha_j < \alpha_{j+1}$. In this way, DL UAV-j recovers the SOI by performing SIC to remove MUI from DL UAV-m for $m > j$, while ignoring MUI from DL UAV-k for $k < j$ [18], [20].

III. Ergodic Capacity Derivations

In this section, ergodic capacity expressions are presented for NOMA-aided multi-UAV communications in the FD-HetNet. The UL and DL ergodic capacity expressions for NOMA-aided multi-UAV communications in a HD-HetNet are also presented as a benchmark.

The ergodic capacity expressions presented in this section are derived based on the work in [44, Lemma 1], where a technique was proposed that enables the ergodic capacity calculation of instantaneous SINRs with both uncorrelated and correlated RVs. The present approach extends this method to evaluate the ergodic capacities of multi-UAV communications in FD-HetNets and HD-HetNets within a stochastic geometry framework.

A. Ergodic Capacity of the MBS in the NOMA-Aided FD-HetNet

The MBS ergodic capacity is defined as $C_{mbs}^{FD} = E\left\{\ln\left(1 + SINR_{mbs}^{FD}\right)\right\}$, where $E\{\bullet\}$ denotes the statistical expectation operator. To evaluate C_{mbs}^{FD}, one will need to employ calculations involving $(2N_U + 4)$-fold numerical integrations to average the PDFs of the associated RVs in $SINR_{mbs}^{FD}$. To avoid such highly intensive computations, one can instead invoke the

[2] By extension, it assumed that the FD-GS has prior knowledge of the locations of the MBS and all UAVs. For the latter, such information can be obtained from flight plans approved by relevant authorities.

[3] The phase noise term γ_ϕ reflects the jitter effect in oscillators due to hardware imperfections [25].

[4] Similar to the FD-GS, it is assumed that all DL UAVs have prior knowledge of the locations of the FD-GS, MBS and surrounding UAVs.

method proposed in [44] that enables a simple evaluation of ergodic capacity.

In the next theorem, we present an exact expression for C_{mbs}^{FD} obtained using the technique in [44].

Theorem 1: The ergodic capacity of the MBS in the FD-HetNet is:

$$C_{mbs}^{FD} = \int_{L_{m,mbs}}^{L_{p,mbs}} \int_0^\infty \frac{\exp(-z)}{z}\left(1 - M_{X_{mbs}}\left(z\rho w_{mbs}^{-n}\right)\right) \times\left(\prod_{i=1}^{N_U}\tau_i\left(z\rho\right)\right) M_{Y_{si,1}}\left(z\rho_{si}\right) M_{Y_{si,2}}\left(z\rho_{si}\right) \times f_{d_{mbs}}(w_{mbs}) dz dw_{mbs}, \quad (5)$$

where $M_X(z)$ is the moment generating function (MGF) of the non-centered Chi-squared distributed RV X, with Rician K factor K_X, which is given as [45, Table. I]:

$$M_X(z) = \frac{1+K_X}{1+K_X+z}\exp\left(\frac{-K_X z}{1+K_X+z}\right), \quad (6)$$

and the function $\tau_i\left(z\rho\right)$ is defined as:

$$\tau_i\left(z\rho\right) = \int_{L_{m,i}}^{L_{p,i}} M_{X_i}\left(z\rho w_i^{-n}\right) f_{d_i}(w_i) dw_i, \quad (7)$$

which averages the MGF $M_{Y_i}\left(z\rho w_i^{-n}\right)$ of interfering UL UAV-i with the PDF $f_{d_i}(w_i)$.

Proof: The proof is provided in Appendix A. ∎

The expression in (5) enables C_{mbs}^{FD} to be evaluated at finite P_t, i.e., ρ, regimes, in the presence of receiver noise and interference, using $(N_U + 2)$-fold numerical integration. In contrast, a direct evaluation of C_{mbs}^{FD} will require $(2N_U + 4)$-fold numerical integrations. [5]

Furthermore, $M_{X_{mbs}}\left(z\rho w_{mbs}^{-n}\right)$ and $\left(\prod_{i=1}^{N_U}\tau_i\left(z\rho\right)\right)$ account for the SOI from the MBS and interference from the UL UAVs, respectively, in (5). Likewise, $M_{Y_{si,1}}\left(z\rho_{si}\right)$ and $M_{Y_{si,2}}\left(z\rho_{si}\right)$ account for the residual SI due to imperfect SI channel estimation and phase noise, respectively, in (5). It should also be noted that C_{mbs}^{FD} in (5) is limited by the number of interfering UL UAVs (N_U) and the strength of the residual SI, i.e., imperfect SI channel estimation (ϵ) and phase noise (γ_ϕ^2). Thus, the ergodic capacity of the MBS at asymptotic P_t regimes, i.e., $C_{mbs,\infty}^{FD}$, can be obtained from (5) as shown in the following corollary.

Corollary 1: The asymptotic ergodic capacity of the MBS in the FD-HetNet is:

$$C_{mbs,\infty}^{FD} = \int_{L_{m,mbs}}^{L_{p,mbs}} \int_0^\infty \frac{1}{z}\left(1 - M_{X_{mbs}}\left(zw_{mbs}^{-n}\right)\right)\left(\prod_{i=1}^{N_U}\tau_i(z)\right) \times M_{Y_{si,1}}(z) M_{Y_{si,2}}(z) f_{d_{mbs}}(w_{mbs}) dz dw_{mbs}. \quad (8)$$

Proof: At asymptotic P_t regimes, $SINR_{mbs}^{FD}$ in (2) reduces to the following instantaneous signal-to-interference ratio (SIR), i.e., SIR_{mbs}^{FD}:

$$SIR_{mbs}^{FD} = \frac{d_{mbs}^{-n} X_{mbs}}{\sum_{i=1}^{N_U} d_i^{-n} X_i + Y_{si,1} + Y_{si,2}}. \quad (9)$$

[5]The expressions presented in this work can be simplified for the special case of Rayleigh fading channels by setting the Rician K factor to be zero. Doing so will yield new expressions for the special case of Rayleigh fading UAV channels, and is left as future extensions of this paper.

Then, evaluating $C_{mbs,\infty}^{FD} = E\left\{\ln\left(1 + SIR_{mbs}^{FD}\right)\right\}$ using the same steps in Appendix A yields (8). This completes the proof. ∎

Similar to (5), $M_{X_{mbs}}\left(z\rho w_{mbs}^{-n}\right)$ and $\left(\prod_{i=1}^{N_U}\tau_i\left(z\rho\right)\right)$ account for the SOI from the MBS and interference from the UL UAVs, respectively, in (8). The functions $M_{Y_{si,1}}\left(z\rho_{si}\right)$ and $M_{Y_{si,2}}\left(z\rho_{si}\right)$ also account for the residual SI due to imperfect SI channel estimation and phase noise in (8), respectively.

From (8), the impact of interference from the UL UAVs can be analyzed within a stochastic geometry framework. Similar to (5), (8) is also influenced by the residual SI at the FD-GS and the number of interfering UL UAVs. Furthermore, scenarios where the detection of the SOI from the MBS is interference-limited can now be identified using (8).

B. Ergodic Capacity of UL UAV-i in the NOMA-Aided FD-HetNet

The ergodic capacity for UL UAV-i is defined as $C_i^{FD} = E\left\{\ln\left(1+SINR_i^{FD}\right)\right\}$. As a direct evaluation of C_i^{FD} requires $(2N_U-2i+4)$-fold numerical integrations, we present an exact expression for C_i^{FD} based on the technique in [44] in the next theorem.

Theorem 2: The ergodic capacity of UL UAV-i in the FD-HetNet is:

$$C_i^{FD} = \int_{L_{m,i}}^{L_{p,i}} \int_0^\infty \frac{\exp(-z)}{z}\left(1 - M_{X_i}\left(z\rho w_i^{-n}\right)\right) \times\left(\prod_{k=i+1}^{N_U}\tau_k\left(z\rho\right)\right) M_{Y_{si,1}}\left(z\rho_{si}\right) M_{Y_{si,2}}\left(z\rho_{si}\right) f_{d_i}(w_i) dz dw_i. \quad (10)$$

Proof: Applying the same technique in Appendix A yields (10), which completes the proof. ∎

Similar to (5), (10) enables the ergodic capacity of UL UAV-i to be evaluated at finite P_t regimes in the presence of receiver noise and interference. Furthermore, (10) is simpler to compute, requiring $(N_U - i + 2)$-fold numerical integrations compared to $(2N_U - 2i + 4)$-fold numerical integrations using direct evaluation.

It should also be emphasized that $M_{X_i}\left(z\rho w_i^{-n}\right)$ and $\left(\prod_{k=i+1}^{N_U}\tau_k\left(z\rho\right)\right)$ account for the SOI from UL UAV-i and interference from the remaining UL UAVs, respectively, in (10). Likewise, $M_{Y_{si,1}}\left(z\rho_{si}\right)$ and $M_{Y_{si,2}}\left(z\rho_{si}\right)$ account for the residual SI due to imperfect SI channel estimation and phase noise, respectively, in (10).

It can be seen from (10) that the remaining number of interfering UL UAVs (N_U) and also the strength of residual SI, i.e., imperfect SI channel estimation (ϵ) and phase noise (γ_ϕ^2), limits C_i^{FD}. When $i \to N_U$, (10) becomes SI-limited due to a diminishing number of interfering UL UAVs. As P_t increases, the asymptotic ergodic capacity of UL UAV-i, i.e., $C_{i,\infty}^{FD}$, can be obtained from (10) as shown in the next corollary.

Corollary 2: The asymptotic ergodic capacity of UL UAV-i in the FD-HetNet is:

$$C_{i,\infty}^{FD} = \int_{L_{m,i}}^{L_{p,i}} \int_0^\infty \frac{1}{z}\left(1 - M_{X_i}\left(zw_i^{-n}\right)\right)\left(\prod_{k=i+1}^{N_U}\tau_k(z)\right) \times M_{Y_{si,1}}(z) M_{Y_{si,2}}(z) f_{d_i}(w_i) dz dw_i. \quad (11)$$

Proof: As P_t increases, $SINR_i^{FD}$ in (3) simplifies into the following instantaneous SIR $\left(SIR_i^{FD}\right)$ expression:

$$SIR_i^{FD} = \frac{d_i^{-n} X_i}{\sum_{k=i+1}^{N_U} d_k^{-n} Y_k + Y_{si,1} + Y_{si,2}}, \quad (12)$$

Then, (11) is obtained by evaluating $C_{i,\infty}^{FD} = E\left\{\ln\left(1 + SIR_i^{FD}\right)\right\}$ using the same steps in Appendix A. This completes the proof. ∎

Similar to (10), $M_{X_i}\left(z\rho w_i^{-n}\right)$, $\left(\prod_{k=i+1}^{N_U} \tau_k(z\rho)\right)$, $M_{Y_{si,1}}(z\rho_{si})$, and $M_{Y_{si,2}}(z\rho_{si})$ account for the SOI from UL UAV-i, interference from the remaining UL UAVs, residual SI due to imperfect SI channel estimation, and residual SI due to phase noise, respectively, in (11). It can be seen from (11) that, apart from residual SI at the FD-GS, interference from the remaining $N_U - i$ UL UAVs can significantly affect the asymptotic ergodic capacity of UL UAV-i when N_U is large. Therefore, (11) can be used to identify a suitable value of N_U when asymptotic ergodic capacity requirements must be satisfied for all UL UAVs.

C. Ergodic Capacity of DL UAV-j in the NOMA-Aided FD-HetNet

The ergodic capacity of DL UAV-j is defined as $C_j^{FD} = E\left\{\ln\left(1 + SINR_j^{FD}\right)\right\}$, which requires $(2 + 2N_U + 2j)$-fold numerical integrations in direct computations. In the following theorem, we invoke the approach in [44] to present an exact expression for C_i^{FD}.

Theorem 3: The ergodic capacity of DL UAV-j in the FD-HetNet is:

$$C_j^{FD} = \int_{L_{m,j}}^{L_{p,j}} \int_0^{\infty} \frac{\exp(-z)}{z} \times \left[M_{X_j}\left(z\rho w_j^{-n} \sum_{k=1}^{j-1} \alpha_k\right) - M_{X_j}\left(z\rho w_j^{-n} \sum_{k=1}^{j} \alpha_k\right)\right] \times \mu_{mbs,j}(z\rho)\left(\prod_{i=1}^{N_U} \mu_{i,j}(z\rho)\right) f_{d_j}(w_j) dz dw_j, \quad (13)$$

where the function $\mu_{x,j}(z\rho), x \in \{mbs, i\}$ is defined as:

$$\mu_{x,j}(z\rho) = \int_{H_{x,j}}^{L_{q,x}} M_{Y_{x,j}}\left(z\rho w_{x,j}^{-n}\right) f_{d_{x,j}}(w_{x,j}|w_j) dw_{x,j} + \int_{L_{q,x}}^{L_{r,x}} M_{Y_{x,j}}\left(z\rho w_{x,j}^{-n}\right) f_{d_{x,j}}(w_{x,j}|w_j) dw_{x,j}, \quad (14)$$

which averages the MGFs of the interfering MBS and UL UAVs ,i.e., $M_{Y_{mbs,j}}\left(z\rho w_{mbs,j}^{-n}\right)$ and $M_{Y_{i,j}}\left(z\rho w_{i,j}^{-n}\right)$, over the respective distance PDFs, i.e., $f_{d_{mbs,j}}(w_{mbs,j}|w_j)$ and $f_{d_{i,j}}(w_{i,j}|w_j)$.

Proof: The proof is given in Appendix B. ∎

The expression in (13) enables a simpler evaluation of the ergodic capacity for DL UAV-j at finite P_t regimes by using $(3 + N_U)$-fold numerical integrations. Furthermore, $\left[M_{X_j}\left(z\rho w_j^{-n} \sum_{k=1}^{j-1} \alpha_k\right) - M_{X_j}\left(z\rho w_j^{-n} \sum_{k=1}^{j} \alpha_k\right)\right]$ accounts for the difference in the strength of the SOI for DL UAV-i and MUI, $\mu_{mbs,j}(z\rho)$ is due to interference from the MBS, and $\left(\prod_{i=1}^{N_U} \mu_{i,j}(z\rho)\right)$ is due to interference from the UL UAVs.

It can also be seen in (13) that the number of interfering UL UAVs (N_U) and the strength of the residual interference $(\beta_{x,j}, x \in \{mbs, i\})$ limits C_j^{FD}. The height of DL UAV-j also influences the strength of the SOI in C_j^{FD} due to the term $M_{X_j}\left(z\rho w_j^{-n} \sum_{k=1}^{j-1} \alpha_k\right) - M_{X_j}\left(z\rho w_j^{-n} \sum_{k=1}^{j} \alpha_k\right)$ in (13). To see this, recall that the power allocation of DL UAV-j (α_j) is determined based on altitude (H_j). Thus, DL UAVs at lower altitudes can remove more MUI than the other DL UAVs at higher altitude, as embodied by $M_{X_j}\left(z\rho w_j^{-n} \sum_{k=1}^{j-1} \alpha_k\right) - M_{X_j}\left(z\rho w_j^{-n} \sum_{k=1}^{j} \alpha_k\right)$.

From (13), it is useful to note that under effective SIC, i.e., $\beta_{x,j} \to 0, x \in \{mbs, i\}$, the impact of interference on C_j^{FD} in (13) is negligible for DL UAV-1. However, for $j > 1$ and $N_D > 1$, C_j^{FD} is limited by interference from the remaining $j-1$ DL UAVs as $P_t \to \infty$. Under such circumstances, the asymptotic ergodic capacity of DL UAV-j $\left(C_{j,\infty}^{FD}\right)$, can be obtained from (13) as shown in the next corollary.

Corollary 3: The asymptotic ergodic capacity of DL UAV-j, for $j > 1$ and $N_D > 1$, in the FD-HetNet is:

$$C_{j,\infty}^{FD} = \int_{L_{m,j}}^{L_{p,j}} \int_0^{\infty} \frac{\exp(-z)}{z} f_{d_j}(w_j) \times \left[M_{X_j}\left(zw_j^{-n} \sum_{k=1}^{j-1} \alpha_k\right) - M_{X_j}\left(zw_j^{-n} \sum_{k=1}^{j} \alpha_k\right)\right] dz dw_j, \quad (15)$$

Proof: When $\beta_{x,j} \to 0, x \in \{mbs, i\}$, $j > 1$, $N_D > 1$ and $P_t \to \infty$, $SINR_j^{FD}$ in (4) can be simplified into the following instantaneous SIR $\left(SIR_j^{FD}\right)$ expression:

$$SIR_j^{FD} = \frac{\alpha_j d_j^{-n} X_j}{d_j^{-n} X_j \sum_{k=1}^{j-1} \alpha_k}. \quad (16)$$

Next, (15) is obtained by evaluating $C_{j,\infty}^{FD} = E\left\{\ln\left(1 + SIR_j^{FD}\right)\right\}$ using the same steps in Appendix B. This completes the proof. ∎

Similar to (13), $\left[M_{X_j}\left(z\rho w_j^{-n} \sum_{k=1}^{j-1} \alpha_k\right) - M_{X_j}\left(z\rho w_j^{-n} \sum_{k=1}^{j} \alpha_k\right)\right]$ accounts for the difference in the strength of the SOI for DL UAV-i and MUI in (15). The expression in (15) also indicates that the quality of NOMA-aided transmissions in the FD-HetNet depends on the quality of the imperfect SIC and strength of the interference from the MBS and UL UAVs. As such, (15) can be used to study tradeoffs between supporting more UL UAVs on the same spectrum and meeting ergodic capacity requirements.

D. Ergodic Capacity of the NOMA-aided HD-HetNet

As a performance benchmark, the NOMA-aided multi-UAV FD-HetNet is compared against a NOMA-aided multi-UAV HD-HetNet in this paper.

In this aspect, it is worth pointing out that similar studies in the literature, e.g., [10], [17], [24], [46], have chosen NOMA-aided HD systems as the performance benchmark. The

TABLE II
SUMMARY OF ADVANTAGES AND DISADVANTAGES FOR VARIOUS NOMA-AIDED FD SCHEMES

Study	Advantages	Disadvantages
[10]	Improves the reliability of downlink NOMA transmissions to the far-user.	Higher equipment cost as it requires a dedicated FD relay. Leads to interference experienced at the near-user.
[17]	Less uplink interference is experienced at the FD relay and downlink users.	Lower spectrum efficiency.
[24]	Less uplink interference experienced at the downlink user.	User scheduling only considers a downlink user at a fixed location. Lower spectrum efficiency.
[46]	Less number of antennas are needed at the FD base station. Lower interference is experienced on each subcarrier.	Higher receiver hardware complexity for each transmitting antenna. Lower spectrum efficiency.
Present Work	Enhanced spectrum efficiency and higher ergodic capacity.	Higher signal processing complexity and delay. Higher transceiver hardware complexity.

main motivation behind such a benchmark comparison is to demonstrate the improved spectrum utilization and associated benefits of NOMA-aided FD systems over NOMA-aided HD systems. When NOMA-aided FD schemes in [10], [17], [24], [46] are compared against the NOMA-aided multi-UAV FD-HetNet in the present work, some observations are noted. For instance, NOMA-aided FD schemes in [10], [17], [24], [46] enable improved reliability and reduced interference in NOMA transmissions at the cost of higher equipment cost and lower spectrum efficiency. In contrast, the NOMA-aided multi-UAV FD-HetNet enable higher spectrum efficiency and ergodic capacity at the cost of higher transceiver hardware complexity, signal processing complexity and delay. A summary of the associated advantages and disadvantages of the various NOMA-aided FD schemes are provided in Table II. While it will be interesting to see how the NOMA-aided multi-UAV FD-HetNet proposed in the present work performs relative to other NOMA-aided FD schemes, such an analysis can be pursued as an extension of the current paper.

In NOMA-aided HD-HetNets, SI is not present as the GS operates in HD mode. As such, the instantaneous SINRs of the MBS $\left(SINR_{mbs}^{HD}\right)$, UL UAVs $\left(SINR_{i}^{HD}\right)$, and DL UAVs $\left(SINR_{j}^{HD}\right)$ are defined as $SINR_{mbs}^{HD} = \frac{\rho d_{mbs}^{-n} X_{mbs}}{1+\rho\sum_{i=1}^{N_U} d_i^{-n} X_i}$, $SINR_{i}^{HD} = \frac{\rho d_i^{-n} X_i}{1+\sum_{k=i+1}^{N_U} \rho d_k^{-n} Y_k}$, and $SINR_{j}^{HD} = \frac{\rho \alpha_j d_j^{-n} X_j}{1+\rho d_j^{-n} X_j \sum_{k=1}^{j-1} \alpha_k}$, respectively.

Then, the ergodic capacity of the MBS, UL UAV-i, and DL UAV-j as respectively defined as $C_{mbs}^{HD} = E\left\{\frac{1}{2}\ln\left(1+SINR_{mbs}^{HD}\right)\right\}$, $C_{i}^{HD} = E\left\{\frac{1}{2}\ln\left(1+SINR_{i}^{HD}\right)\right\}$, and $C_{j}^{HD} = E\left\{\frac{1}{2}\ln\left(1+SINR_{j}^{HD}\right)\right\}$. In the following theorem, exact expressions are presented for C_{mbs}^{HD}, C_{i}^{HD}, and C_{j}^{HD}.

Theorem 4: The ergodic capacity of the MBS, UL UAV-i, and DL UAV-j in the HD-HetNet are given in (17), (18), and (19), respectively.

$$C_{mbs}^{HD} = \frac{1}{2}\int_{L_{m,mbs}}^{L_{p,mbs}}\int_{0}^{\infty}\frac{\exp(-z)}{z}\left(1-M_{X_{mbs}}\left(z\rho w_{mbs}^{-n}\right)\right)\times\left(\prod_{i=1}^{N_U}\tau_i(z\rho)\right)f_{d_{mbs}}(w_{mbs})dzdw_{mbs}, \quad (17)$$

$$C_{i}^{HD} = \frac{1}{2}\int_{L_{m,i}}^{L_{p,i}}\int_{0}^{\infty}\frac{\exp(-z)}{z}\left(1-M_{X_i}\left(z\rho w_{i}^{-n}\right)\right)\times\left(\prod_{k=i+1}^{N_U}\tau_k(z\rho)\right)f_{d_i}(w_i)dzdw_i, \quad (18)$$

$$C_{j}^{HD} = \frac{1}{2}\int_{L_{m,j}}^{L_{p,j}}\int_{0}^{\infty}\frac{\exp(-z)}{z}f_{d_j}(w_j)\times\left[M_{X_j}\left(z\rho w_j^{-n}\sum_{k=1}^{j-1}\alpha_k\right)-M_{X_j}\left(z\rho w_j^{-n}\sum_{k=1}^{j}\alpha_k\right)\right]dzdw_j. \quad (19)$$

Proof: The expressions for (17) and (18) are obtained using the same steps in Appendix A while (19) is obtained using the same method in Appendix B. This completes the proof. ■

For (17), $M_{X_{mbs}}\left(z\rho w_{mbs}^{-n}\right)$ and $\left(\prod_{i=1}^{N_U}\tau_i(z\rho)\right)$ account for the SOI from the MBS and interference from the UL UAVs, respectively. For (18), $M_{X_i}\left(z\rho w_i^{-n}\right)$ and $\left(\prod_{k=i+1}^{N_U}\tau_k(z\rho)\right)$ account for the SOI from UL UAV-i and interference from the remaining UL UAVs, respectively. Finally, $\left[M_{X_j}\left(z\rho w_j^{-n}\sum_{k=1}^{j-1}\alpha_k\right)-M_{X_j}\left(z\rho w_j^{-n}\sum_{k=1}^{j}\alpha_k\right)\right]$ account for the difference in the strength of the SOI for DL UAV-i and MUI in (19).

From Theorem 4, the ergodic capacity of the MBS and UL UAV-$i, 1 \le i \le N_U - 1$ are interference-limited at high P_t regimes due to the presence of interference from other UL UAVs. Likewise, the ergodic capacity of DL UAV-j when $j > 1$ is also interference-limited at high P_t regimes due to MUI from the DL UAVs. To this end, we present the asymptotic ergodic capacity of the MBS $\left(C_{mbs,\infty}^{HD}\right)$, UL UAV-$i$ $\left(C_{i,\infty}^{HD}\right)$, and DL UAV-$j$ $\left(C_{j,\infty}^{HD}\right)$ using (17), (18), and (19), respectively, as shown in the following corollary.

Corollary 4: The asymptotic ergodic capacity of the MBS, UL UAV-i, and DL UAV-j in the HD-HetNet are given in (20), (21), and (22), respectively, for $i \le N_U - 1$ and $j > 1$.

$$C_{mbs,\infty}^{HD} = \frac{1}{2}\int_{L_{m,mbs}}^{L_{p,mbs}}\int_{0}^{\infty}\frac{1}{z}\left(1-M_{X_{mbs}}\left(zw_{mbs}^{-n}\right)\right)\times\left(\prod_{i=1}^{N_U}\tau_i(z)\right)f_{d_{mbs}}(w_{mbs})dzdw_{mbs}, \quad (20)$$

$$C_{i,\infty}^{HD} = \frac{1}{2}\int_{L_{m,i}}^{L_{p,i}}\int_{0}^{\infty}\frac{1}{z}\left(1-M_{X_i}\left(zw_{i}^{-n}\right)\right)\times\left(\prod_{k=i+1}^{N_U}\tau_k(z)\right)f_{d_i}(w_i)dzdw_i, \quad (21)$$

$$C_{j,\infty}^{HD} = \frac{1}{2}\int_{L_{m,j}}^{L_{p,j}}\int_{0}^{\infty}\frac{\exp(-z)}{z}f_{d_j}(w_j)\times\left[M_{X_j}\left(zw_j^{-n}\sum_{k=1}^{j-1}\alpha_k\right)-M_{X_j}\left(zw_j^{-n}\sum_{k=1}^{j}\alpha_k\right)\right]dzdw_j. \quad (22)$$

Proof: The expressions in (20), (21), and (22) are obtained through the same techniques seen in Corollaries 1, 2, and 3, respectively. This completes the proof. ■

Similar to Theorem 4, $M_{X_{mbs}}\left(z\rho w_{mbs}^{-n}\right)$ and $\left(\prod_{i=1}^{N_U}\tau_i(z\rho)\right)$ account for the SOI from the MBS and interference from the UL UAVs, respectively, in (20). For (21), $M_{X_i}\left(z\rho w_i^{-n}\right)$ and $\left(\prod_{k=i+1}^{N_U}\tau_k(z\rho)\right)$ account for the SOI from UL UAV-i and interference from the remaining UL UAVs, respectively. Finally, $\left[M_{X_j}\left(z\rho w_j^{-n}\sum_{k=1}^{j-1}\alpha_k\right)-M_{X_j}\left(z\rho w_j^{-n}\sum_{k=1}^{j}\alpha_k\right)\right]$ account for the difference in the strength of the SOI for DL UAV-i and MUI in (22).

Unlike in FD-HetNets, UL and DL transmissions in HD-HetNets cannot concurrently occur on the same spectrum as separate spectrum bands or timeslots, i.e., time-frequency resource blocks, are required. To account for the orthogonality of time-frequency resource blocks in HD-HetNets, a factor of $\frac{1}{2}$ is introduced in (20), (21) and (22). Doing so enables a fair comparison between HD-HetNets and FD-HetNets.

E. Ergodic Capacity Gains of NOMA-aided FD-HetNets over HD-HetNets

Although HD-HetNets inherently experience less interference than FD-HetNets, a much higher throughput can still be achieved by the latter. In particular, ergodic capacity gains can be achieved FD-HetNets with effective interference management and also through the higher number of UAVs that can be concurrently supported on the same spectrum.

To this end, quantifying the ergodic capacity gain of NOMA-aided multi-UAV communications in FD-HetNets over HD-HetNets is of practical significance for system designers. Let the ergodic capacity gain of the MBS, UL UAV-i, and DL UAV-j be defined as $\Delta_{mbs}=C_{mbs}^{FD}-C_{mbs}^{HD}$, $\Delta_i=C_i^{FD}-C_i^{HD}$, and $\Delta_j=C_j^{FD}-C_j^{HD}$, respectively. Then, from Theorems 1, 2, 3, and 4, we present exact expressions for $\Delta_x, x\in\{mbs,i,j\}$ in the next corollary.

Corollary 5: The ergodic capacity gains of the MBS, UL UAV-i, and DL UAV-j in the FD-HetNet over the HD-HetNet are given in (23), (24), and (25), respectively.

$$\begin{aligned}\Delta_{mbs} &= \int_{L_{m,mbs}}^{L_{p,mbs}}\int_0^{\infty}\frac{\exp(-z)}{z}\left(1-M_{X_{mbs}}\left(z\rho w_{mbs}^{-n}\right)\right)\\ &\quad\times\left(\prod_{i=1}^{N_U}\tau_i(z\rho)\right)\left(M_{Y_{si,1}}(z\rho_{si})M_{Y_{si,2}}(z\rho_{si})-\frac{1}{2}\right)\\ &\quad\times f_{d_{mbs}}(w_{mbs})dzdw_{mbs}, \quad (23)\\ \Delta_i &= \int_{L_{m,i}}^{L_{p,i}}\int_0^{\infty}\frac{\exp(-z)}{z}\left(1-M_{X_i}\left(z\rho w_i^{-n}\right)\right)\\ &\quad\times\left(\prod_{k=i+1}^{N_U}\tau_k(z\rho)\right)\left(M_{Y_{si,1}}(z\rho_{si})M_{Y_{si,2}}(z\rho_{si})-\frac{1}{2}\right)\\ &\quad\times f_{d_i}(w_i)dzdw_i, \quad (24)\\ \Delta_j &= \int_{L_{m,j}}^{L_{p,j}}\int_0^{\infty}\frac{\exp(-z)}{z}\\ &\quad\times\left[M_{X_j}\left(z\rho w_j^{-n}\sum_{k=1}^{j-1}\alpha_k\right)-M_{X_j}\left(z\rho w_j^{-n}\sum_{k=1}^{j}\alpha_k\right)\right]\end{aligned}$$

TABLE III
SIMULATION PARAMETERS

Parameter	Value
Number of UAVs	$N_U\in\{3,4,5,6\}, N_D\in\{3,4,5,6\}$ [3], [47]
Rician K Factors	10 dB [11, Table V]
Transmit Power	0 dBm $\le P_t \le$ 30 dBm [47]
Carrier Frequency	f_c = 2 GHz [47]
Bandwidth	B_W = 20 MHz [47]
Phase Noise	$\gamma_\phi^2\in\{-130$ dBm, -140 dBm$\}$ [7], [37], [38]
SI Channel Estimation Error	$\epsilon\in\{0.5, 0.1, 0.01\}$ [7], [37], [38]
Radius	r_a = 10 km [39]
MBS Antenna Height	H_{mbs} = 0.03 km [47]
Minimum UAV Altitude	$H_{min}\in\{0.1,1\}$ km [47]
Altitude Separation Factor	$\omega\in\{0.1,1\}$
Residual Interference	$\beta_{mbs,j},\beta_{i,j}\in\{0,(0.04)^3,(0.07)^3\}$ [17]
Pathloss Exponent	n = 2 [11, Table III], [33]

$$\times\left(\mu_{mbs,j}(z\rho)\left(\prod_{i=1}^{N_U}\mu_{i,j}(z\rho)\right)-\frac{1}{2}\right)f_{d_j}(w_j)dzdw_j. \quad (25)$$

Proof: The proof is provided in Appendix C. ■

The ergodic capacity gain expressions given in (23), (24), and (25) can be used to determine scenarios where the FD-HetNet is able to achieve higher ergodic capacity than the HD-HetNet. In particular, $\Delta_x<0, x\in\{mbs,i,j\}$ indicates that node x in the FD-HetNet achieves lower ergodic capacity than the HD-HetNet. Similarly, $\Delta_x>0, x\in\{mbs,i,j\}$ indicates that node x achieves a higher ergodic capacity in the FD-HetNet than the HD-HetNet.

It is also worth emphasizing that $\Delta_x, x\in\{mbs,i,j\}$ can be used to provide system design guidelines. For instance, Δ_{mbs} and Δ_i can be negative due to the term $M_{Y_{si,1}}(z\rho_{si})M_{Y_{si,2}}(z\rho_{si})-\frac{1}{2}$ in (23) and (24), respectively. To illustrate this, it can be seen that increasing SI channel estimation errors (ϵ), i.e., reducing SI cancellation, or phase noise (γ_ϕ^2) leads to $M_{Y_{si,1}}(z\rho_{si})M_{Y_{si,2}}(z\rho_{si})\to 0$. Likewise, Δ_j can also be negative due to the term $\mu_{mbs,j}(z\rho)\left[\prod_{i=1}^{N_U}\mu_{i,j}(z\rho)\right]-\frac{1}{2}$ in (25). Specifically, $\mu_{mbs,j}(z\rho)\left[\prod_{i=1}^{N_U}\mu_{i,j}(z\rho)\right]\to 0$ as residual interference ($\beta_{x,j}, x\in\{mbs,i\}$) increases. Therefore, the expressions given in (23), (24), and (25) can be used to identify crucial system parameters, e.g., transmit power (P_t), SI channel estimation error (ϵ) or bandwidth (B_W), that enables the FD-HetNet an advantageous ergodic capacity gain over HD-HetNets while meeting operational constraints.

IV. NUMERICAL RESULTS

Numerical results pertaining to the ergodic capacity and ergodic sum capacity of NOMA-aided multi-UAV communications in the FD-HetNet and HD-HetNet are presented in this section. For the FD-HetNet and HD-HetNet, the ergodic sum capacity is defined as $C_{sum}^{FD}=C_{mbs}^{FD}+\sum_{i=1}^{N_U}C_i^{FD}+\sum_{j=1}^{N_D}C_j^{FD}$ and $C_{sum}^{HD}=C_{mbs}^{HD}+\sum_{i=1}^{N_U}C_i^{HD}+\sum_{j=1}^{N_D}C_j^{HD}$, respectively. Likewise, ergodic sum capacity gain for UL and DL transmissions are defined as $\Delta_{UL}=\Delta_{mbs}+\sum_{i=1}^{N_U}\Delta_i$ and $\Delta_{DL}=\sum_{j=1}^{N_D}\Delta_j$, respectively. We also present Monte Carlo simulation results conducted with 10^5 samples on MATLAB, and numerical results obtained from Mathematica, using parameters that are

provided in Table III. [6]

A. Ergodic Capacity at the FD-GS and DL UAVs

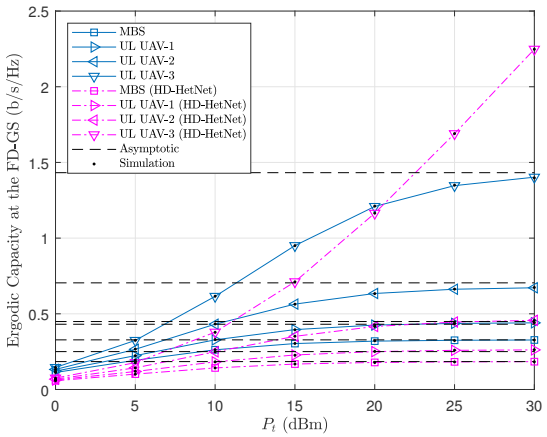

(a) Ergodic Capacity at the FD-GS.

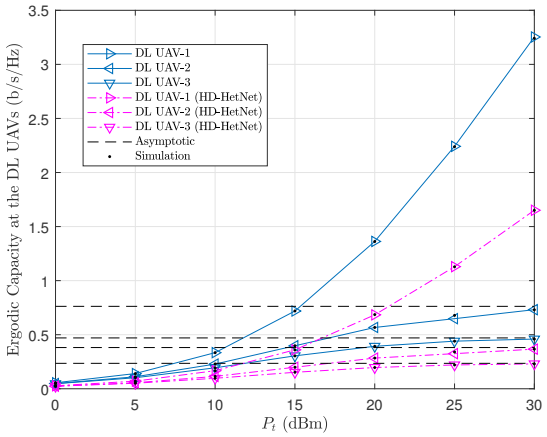

(b) Ergodic Capacity at the DL UAVs.

Fig. 2. Ergodic capacity comparison at the FD-GS and DL UAVs in the NOMA-aided FD-HetNet for $N_U = N_D = 3$, $H_{min} = 0.1$ km, $\omega = 0.1$, $\gamma_\phi^2 = -130$ dBm, $\epsilon = 0.01$, and $\beta_{mbs,j} = \beta_{i,j} = (0.04)^3$.

The ergodic capacity at the FD-GS is plotted in Fig. 2a for the MBS $\left(C_{mbs}^{FD}\right)$ and UL UAV-i $\left(C_i^{FD}\right)$. Likewise, the ergodic capacity at the DL UAVs $\left(C_j^{FD}\right)$ is plotted in Fig. 2b. As a benchmark, the ergodic capacities of the MBS $\left(C_{mbs}^{HD}\right)$, UL UAV-$i$ $\left(C_i^{HD}\right)$, and DL UAV-j $\left(C_j^{HD}\right)$ are plotted for the NOMA-aided HD-HetNet.

Despite the FD-GS experiencing residual SI and MUI from the UL UAVs, it is observed from Fig. 2a that $C_{mbs}^{FD} > C_{mbs}^{HD}$ and $C_i^{FD} > C_i^{HD}, i \in \{1,2\}$ for 0 dBm $\leq P_t \leq$ 30 dBm. Such an observation is due to effective SI mitigation and MUI from the UL UAVs, resulting in $SINR_{mbs}^{FD} > SINR_{mbs}^{HD}$ and $SINR_i^{FD} > SINR_i^{HD}$. Moreover, Corollaries 1 and 2 are confirmed, since $C_{mbs}^{FD} \approx C_{mbs,\infty}^{FD}$ and $C_i^{FD} \approx C_{i,\infty}^{FD}$ at high P_t regimes. For the case of UL UAV-3, strong residual SI at the FD-GS is experienced at high P_t regimes, leading to $C_3^{FD} < C_3^{HD}$.

In Fig. 2b, it is observed that $C_j^{FD} > C_j^{HD}$ for 0 dBm $\leq P_t \leq$ 30 dBm. Furthermore, at high P_t regimes, Corollary 3 is confirmed since $C_j^{FD} \approx C_{j,\infty}^{HD}, j \in \{2,3\}$. Specifically, it is observed that $C_j^{FD}, j \in \{2,3\}$ begins to plateau. Such a trend is due to the fact that the instantaneous SINR at DL UAV-$j, j \in \{2,3\}$, i.e., $SINR_j^{FD}$ becomes largely limited by MUI from the preceding $j-1$ DL UAVs, which cannot be canceled due to the nature of the SIC ordering.

From Fig. 2, it is demonstrated that having the GS operate in FD mode, i.e., FD-HetNet, enables higher ergodic capacity over the HD-GS to be attained for the MBS, UL UAVs, and DL UAVs.

B. Impact of Height on Ergodic Sum Capacity

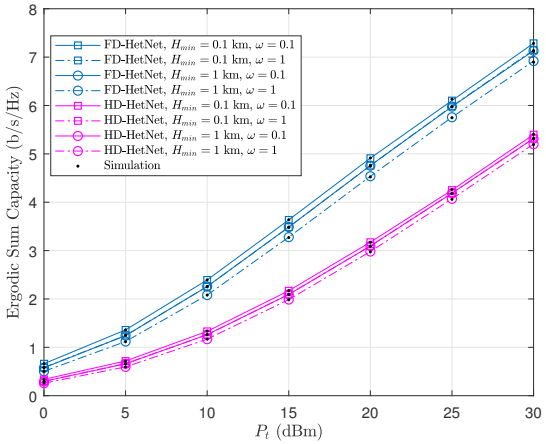

Fig. 3. Impact of height on the ergodic sum capacity of the NOMA-aided FD-HetNet and HD-HetNet for $N_U = N_D = 3$, $\gamma_\phi^2 = -130$ dBm, $\epsilon = 0.01$, and $\beta_{mbs,j} = \beta_{i,j} = (0.04)^3$.

Fig. 3 shows the impact of height on the ergodic sum capacity for the FD-HetNet and HD-HetNet. It can be seen that the ergodic sum capacity of the FD-HetNet $\left(C_{sum}^{FD}\right)$ and HD-HetNet $\left(C_{sum}^{HD}\right)$ exhibit similar trends, with $C_{sum}^{FD} > C_{sum}^{HD}$ for 0 dBm $\leq P_t \leq$ 30 dBm. When the minimum UAV altitude $\left(H_{min}\right)$ is low and the altitude separation factor (ω) is small, a higher $C_{sum}^x, x \in \{FD, HD\}$ is observed. Correspondingly, it is seen that a higher H_{min} and larger ω leads to a lower $C_{sum}^x, x \in \{FD, HD\}$.

The reasons behind the observations in Fig. 3 are due to the fact that increasing H_{min} causes the UL and DL UAVs to be operating at a higher altitude. In turn, the SOIs of UL UAV-i and the GS become weaker at the receiving GS and DL UAV-j, respectively, i.e., weaker SINRs. Similarly, increasing ω results in a larger separating altitude between all UAVs, i.e., higher operating altitude for all UAVs, leading to weaker SINR at the FD-GS and the DL UAVs. However, a larger ω also results in weaker MUI at the receiving GS and DL UAVs.

When SIC detection is employed at the GS and DL UAV-j, MUI from the UAVs can be effectively managed. Hence, both the FD-HetNet and HD-HetNet are able to have the UL and

[6]To obtain the simulated ergodic capacity of the UAVs and MBS, the RVs present in the various SINR expressions are first generated in MATLAB. Thereafter, using the ergodic capacity definitions, the generated RVs are used to compute the various average ergodic capacities. While it will be interesting to see how such simulations can be done using an event-driven simulator, e.g., ns-2 or OMNeT++, the analytical and simulation framework in this direction of work is left as future extensions of this paper.

DL UAVs operate a lower H_{min} and smaller ω while achieving higher $C_{sum}^{x}, x \in \{FD, HD\}$, leading to the trend in Fig. 3.

C. Impact of the Number of Deployed UAVs on Ergodic Sum Capacity

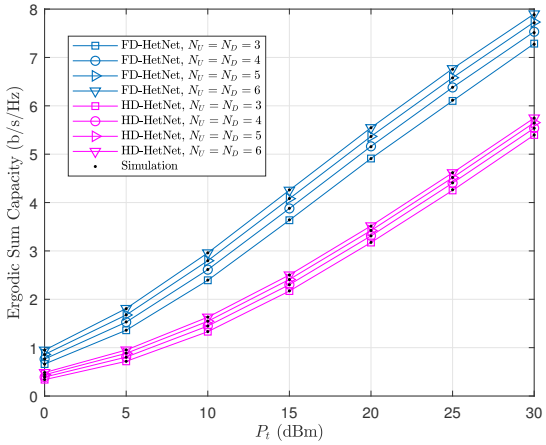

Fig. 4. Impact of the number of deployed UAVs on the ergodic sum capacity of the NOMA-aided FD-HetNet and HD-HetNet for H_{min} = 0.1 km, ω = 0.1, $\gamma_{\phi}^2 = -130$ dBm, $\epsilon = 0.01$, and $\beta_{mbs,j} = \beta_{i,j} = (0.04)^3$.

The impact of the number of deployed UAVs on the ergodic sum capacity for the FD-HetNet and HD-HetNet is plotted in Fig. 4. It can be observed from Fig. 4 that increasing N_U and N_D leads to higher ergodic sum capacity $\left(C_{sum}^{x}, x \in \{FD, HD\}\right)$ for both FD-HetNet and HD-HetNet. Such an observation is due effective interference cancellation at the GS and DL UAVs. Specifically, SIC detectors are employed at the GS and DL UAVs. Hence, MUI from the UAVs can be effectively mitigated in the FD-HetNet and HD-HetNet. As a consequence, more UL and DL UAVs can be supported.

It is also useful to note that in HD-HetNets, the MBS and UL UAVs communicate on time-frequency resource blocks that are orthogonal to those allocated for DL UAVs. In contrast, the FD-GS enables the MBS, UL UAVs and DL UAVs to communicate over the same time-frequency resource block. As a result, increasing N_U and N_D leads to a higher increase in C_{sum}^{FD} than in C_{sum}^{HD}, which in turn leads to $C_{sum}^{FD} > C_{sum}^{HD}$ for 0 dBm $\leq P_t \leq$ 30 dBm.

Therefore, Fig. 4 highlights the potential for FD-HetNets to address spectrum scarcity in UAV communications.

D. Impact of SI Cancellation, Phase Noise, and Residual Interference on Ergodic Sum Capacity

The impact of SI cancellation (ϵ) and phase noise (γ_{ϕ}^2) on the FD-HetNet ergodic sum capacity $\left(C_{sum}^{FD}\right)$ is shown in Fig. 5. To begin, it is useful to recall that SI cancellation is computed as $1/(\epsilon\sigma^2)$ [37], [40]. Thus, increasing $\epsilon = 0.01$ to $\epsilon = 0.1$ also increases the SI channel estimation error while leading to a lower level of SI cancellation at the FD-GS. Consequently, the resultant instantaneous SINR of the MBS $\left(SINR_{mbs}^{FD}\right)$ and UL UAV-i $\left(SINR_{i}^{FD}\right)$ at the FD-GS becomes limited by residual SI. Similarly, increasing γ_{ϕ}^2 also causes the strength of the residual SI to increase. However, as $\gamma_{\phi}^2 < \sigma^2$,

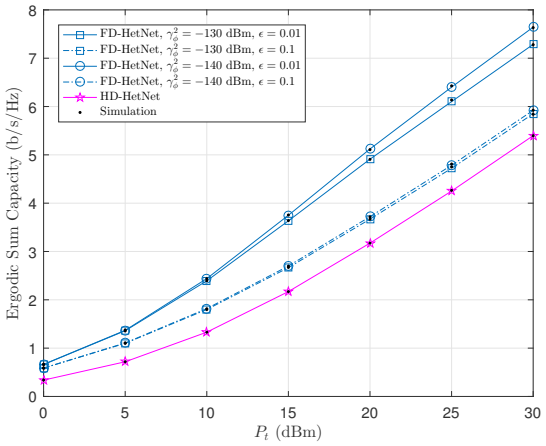

Fig. 5. Impact of SI cancellation and phase noise on the ergodic sum capacity of the NOMA-aided FD-HetNet for $N_U = N_D = 3$, $H_{min} = 0.1$ km, $\omega = 0.1$, and $\beta_{mbs,j} = \beta_{i,j} = (0.04)^3$.

changes in ϵ have more significant impact on the FD-GS as the residual SI may be above the noise floor. Thus, as seen in Fig. 5, decreasing ϵ, i.e., increasing SI cancellation, elicits a higher C_{sum}^{FD} than reducing γ_{ϕ}^2.

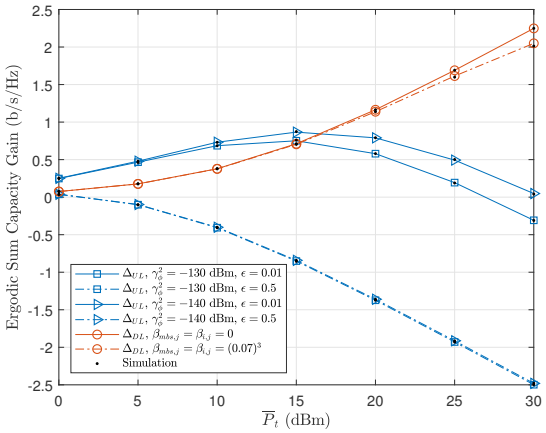

Fig. 6. Impact of SI cancellation, phase noise, and residual interference on the ergodic sum capacity gain of the NOMA-aided FD-HetNet for $N_U = N_D = 3$, $H_{min} = 0.1$ km, and $\omega = 0.1$.

Fig. 6 shows the impact of SI cancellation, phase noise, and residual interference $(\beta_{x,j}, x \in \{mbs, i\})$ on the ergodic capacity gain for UL and DL transmissions, i.e., Δ_{UL} and Δ_{DL}. As explained earlier, increasing ϵ leads to a more drastic drop in Δ_{UL} than increasing γ_{ϕ}^2, as seen in Fig. 6. Furthermore, a slight increase in $\beta_{mbs,j}$ and $\beta_{i,j}$ also leads to a drop in Δ_{DL} as the DL UAVs become limited by residual interference at high P_t regimes. Therefore, Corollary 5 is confirmed in Fig. 6.

It is worth emphasizing that the analysis in this paper assumes SI cancellation levels of 137 dB ($\epsilon = 0.5$) to 154 dB ($\epsilon = 0.01$). Such SI cancellation levels have been reported in [48], where SI cancellation beyond 150 dB was noted. Therefore, Fig. 5 and Fig. 6 highlights the feasibility of achieving practical FD-HetNets for NOMA-aided multi-UAV communications.

V. Conclusion

NOMA-aided multi-UAV communications in FD-HetNets is proposed in this paper as a pragmatic and attractive solution to address spectrum scarcity in UAV communications. Through an analysis of the ergodic capacity within a BPP-based stochastic geometry framework, it is shown that higher ergodic capacities are attained by the MBS and UAVs in the FD-HetNet. In addition, the FD-HetNet allows more UAVs to be at lower altitudes while achieving a higher ergodic sum capacity and ergodic capacity gains over HD-HetNets. Finally, it is demonstrated that NOMA-aided multi-UAV communications in FD-HetNet achieves higher ergodic sum capacity over HD-HetNets despite weaker SI suppression and stronger phase noise. Thus, the feasibility of addressing spectrum scarcity in UAV communications is highlighted.

Acknowledgment

This research is jointly funded by Airbus Singapore Pte Ltd and the Singapore Economic Development Board (EDB).

Appendix A
Proof of Theorem 1

From [44, eq. (5)], the instantaneous ergodic capacity of the MBS in the FD-HetNet can be written as:

$$\begin{aligned}\ln\left(1+SINR_{mbs}^{FD}\right) &= \int_0^{\infty}\frac{\exp(-z)}{z}\left[1-\exp\left(-z\rho d_{mbs}^{-n}X_{mbs}\right)\right]\\ &\times\exp\left(-z\left(\rho\sum_{i=1}^{N_U}d_i^{-n}X_i+\rho_{si}Y_{si,1}+\rho_{si}Y_{si,2}\right)\right)dz. \quad (26)\end{aligned}$$

Thereafter, the ergodic capacity C_{mbs}^{FD} conditioned on d_{mbs} and d_i can be given as:

$$\begin{aligned}E\left\{\ln\left(1+SINR_{mbs}^{FD}\right)\middle|d_{mbs},d_i\right\} &= \int_0^{\infty}\frac{\exp(-z)}{z}\left(1-M_{X_{mbs}}\left(z\rho d_{mbs}^{-n}\right)\right)\\ &\times\left(\prod_{i=1}^{N_U}M_{X_i}\left(z\rho d_i^{-n}\right)\right)M_{Y_{si,1}}\left(z\rho_{si}\right)M_{Y_{si,2}}\left(z\rho_{si}\right)dz. \quad (27)\end{aligned}$$

Averaging (27) over the PDFs of d_{mbs} and d_i yields (5). This completes the proof.

Appendix B
Proof of Theorem 3

From (4), $SINR_j^{FD}$ comprises uncorrelated RVs, i.e., $Y_{i,j}$ and $Y_{mbs,j}$, and a correlated RV X_j. Using [44, eq. (5)], the instantaneous ergodic capacity of DL UAV-j in the FD-HetNet is:

$$\begin{aligned}\ln\left(1+SINR_j^{FD}\right) &= \int_0^{\infty}\frac{\exp(-z)}{z}\\ &\times\left[\exp\left(-z\frac{\rho}{d_j^n}X_j\sum_{k=1}^{j-1}\alpha_k\right)-\exp\left(-z\frac{\rho}{d_j^n}X_j\sum_{k=1}^{j}\alpha_k\right)\right]\\ &\times\exp\left(-z\rho\left[d_{mbs,j}^{-n}Y_{mbs,j}+\sum_{i=1}^{N_U}d_{i,j}^{-n}Y_{i,j}\right]\right)dz, \quad (28)\end{aligned}$$

From (28), the ergodic capacity C_j^{FD} conditioned on d_j, $d_{i,j}$, and $d_{mbs,j}$ is:

$$\begin{aligned}E\left\{\ln\left(1+SINR_j^{FD}\right)\middle|d_j,d_{i,j},d_{mbs,j}\right\} &= \int_0^{\infty}\frac{\exp(-z)}{z}\left[M_{X_j}\left(z\frac{\rho}{d_j^n}\sum_{k=1}^{j-1}\alpha_k\right)-M_{X_j}\left(z\frac{\rho}{d_j^n}\sum_{k=1}^{j}\alpha_k\right)\right]\\ &\times M_{Y_{mbs,j}}\left(z\rho d_{mbs,j}^{-n}\right)\left(\prod_{i=1}^{N_U}M_{Y_{i,j}}\left(z\rho d_{i,j}^{-n}\right)\right)dz, \quad (29)\end{aligned}$$

Subsequently, averaging (29) over the PDFs of d_j, $d_{i,j}$, and $d_{mbs,j}$ yields:

$$\begin{aligned}E\left\{\ln\left(1+SINR_j^{FD}\right)\right\} &= \int_{L_{m,j}}^{L_{p,j}}\int_0^{\infty}\frac{\exp(-z)}{z}\\ &\times\left[M_{X_j}\left(z\frac{\rho}{w_j^n}\sum_{k=1}^{j-1}\alpha_k\right)-M_{X_j}\left(z\frac{\rho}{w_j^n}\sum_{k=1}^{j}\alpha_k\right)\right]\\ &\times\left(\int_{H_{mbs,j}}^{L_{q,mbs}}M_{Y_{mbs,j}}\left(z\rho w_{mbs,j}^{-n}\right)f_{d_{mbs,j}}(w_{mbs,j}|w_j)dw_{mbs,j}\right.\\ &\left.+\int_{L_{q,mbs}}^{L_{r,mbs}}M_{Y_{mbs,j}}\left(z\rho w_{mbs,j}^{-n}\right)f_{d_{mbs,j}}(w_{mbs,j}|w_j)dw_{mbs,j}\right)\\ &\times\left(\prod_{i=1}^{N_U}\left[\int_{H_{i,j}}^{L_{q,i}}M_{Y_{i,j}}\left(z\rho w_{i,j}^{-n}\right)f_{d_{i,j}}(w_{i,j}|w_j)dw_{i,j}\right.\right.\\ &\left.\left.+\int_{L_{q,i}}^{L_{r,i}}M_{Y_{i,j}}\left(z\rho w_{i,j}^{-n}\right)f_{d_{i,j}}(w_{i,j}|w_j)dw_{i,j}\right]\right)f_{d_j}(w_j)dzdw_j. \quad (30)\end{aligned}$$

Thereafter, (13) is obtained after simplifying (30). This completes the proof.

Appendix C
Proof of Corollary 5

Starting with Δ_{mbs}, the exact expression can be written in terms of C_{mbs}^{FD} in (5) and C_{mbs}^{HD} in (17) as:

$$\begin{aligned}\Delta_{mbs} &= C_{mbs}^{FD}-C_{mbs}^{HD}\\ &= \int_{L_{m,mbs}}^{L_{p,mbs}}\int_0^{\infty}\frac{\exp(-z)}{z}\left(1-M_{X_{mbs}}\left(z\rho w_{mbs}^{-n}\right)\right)\\ &\times\left(\prod_{i=1}^{N_U}\tau_i(z\rho)\right)M_{Y_{si,1}}(z\rho_{si})M_{Y_{si,2}}(z\rho_{si})\\ &\times f_{d_{mbs}}(w_{mbs})dzdw_{mbs}\\ &-\frac{1}{2}\int_{L_{m,mbs}}^{L_{p,mbs}}\int_0^{\infty}\frac{\exp(-z)}{z}\left(1-M_{X_{mbs}}\left(z\rho w_{mbs}^{-n}\right)\right)\\ &\times\left(\prod_{i=1}^{N_U}\tau_i(z\rho)\right)f_{d_{mbs}}(w_{mbs})dzdw_{mbs}. \quad (31)\end{aligned}$$

Thereafter, (23) is obtained after some algebraic simplification. The exact expressions for Δ_i and Δ_j are also obtained in the same manner. This completes the proof.

REFERENCES

[1] A. Yadav, G. I. Tsiropoulos, and O. A. Dobre, "Full-duplex communications: Performance in ultradense mm-wave small-cell wireless networks," *IEEE Veh. Technol. Mag.*, vol. 13, no. 2, pp. 40–47, June 2018.

[2] Q. Wu and R. Zhang, "Common throughput maximization in UAV-enabled OFDMA systems with delay consideration," *IEEE Trans. Commun.*, vol. 66, no. 12, pp. 6614–6627, December 2018.

[3] X. Wang, H. Zhang, Y. Tian, and V. C. Leung, "Modeling and Analysis of Aerial Base Station-Assisted Cellular Networks in Finite Areas Under LoS and NLoS Propagation," *IEEE Trans. Wireless Commun.*, vol. 17, no. 10, pp. 6985–7000, October 2018.

[4] S. Enayati, H. Saeedi, H. Pishro-Nik, and H. Yanikomeroglu, "Moving aerial base station networks: Stochastic geometry analysis and design perspective," *IEEE Trans. Wireless Commun.*, 2019.

[5] W. Fawaz, C. Abou-Rjeily, and C. Assi, "UAV-aided cooperation for FSO communication systems," *IEEE Commun. Mag.*, vol. 56, no. 1, pp. 70–75, 2018.

[6] V. V. Chetlur and H. S. Dhillon, "Downlink coverage analysis for a finite 3-d wireless network of unmanned aerial vehicles," *IEEE Trans. Commun*, vol. 65, no. 10, pp. 4543–4558, 2017.

[7] T. Z. H. Ernest, A. S. Madhukumar, R. P. Sirigina, and A. K. Krishna, "A Hybrid-Duplex System with Joint Detection for Interference-Limited UAV Communications," *IEEE Trans. Veh. Technol.*, Jan. 2019.

[8] ——, "An Outage Probability Analysis of Full-Duplex NOMA in UAV Communications," in *Proc. IEEE Wireless Commun. Netw. Conf. (WCNC)*, Marrakech, Morocco, 2019, pp. 1–5.

[9] ——, "A Power Series Approach for Hybrid-Duplex UAV Communication Systems under Rician Shadowed Fading," *IEEE Access*, 2019.

[10] T. M. C. Chu and H.-J. Zepernick, "Performance of a non-orthogonal multiple access system with full-duplex relaying," *IEEE Commun. Lett.*, vol. 22, no. 10, pp. 2084–2087, October 2018.

[11] D. W. Matolak and R. Sun, "Air-ground channel characterization for unmanned aircraft systems part iii: The suburban and near-urban environments," *IEEE Trans. Veh. Technol*, 2017.

[12] R. Sun and D. W. Matolak, "Air–ground channel characterization for unmanned aircraft systems part ii: Hilly and mountainous settings," *IEEE Trans. Veh. Technol*, vol. 66, no. 3, pp. 1913–1925, 2017.

[13] H. Hellaoui, O. Bekkouche, M. Bagaa, and T. Taleb, "Aerial control system for spectrum efficiency in uav-to-cellular communications," *IEEE Commun. Mag.*, vol. 56, no. 10, pp. 108–113, October 2018.

[14] Y. Liu, Z. Qin, Y. Cai, Y. Gao, G. Y. Li, and A. Nallanathan, "UAV communications based on non-orthogonal multiple access," *IEEE Wireless Commun.*, vol. 26, no. 1, pp. 52–57, 2019.

[15] Z. Yang, Z. Ding, P. Fan, and N. Al-Dhahir, "A general power allocation scheme to guarantee quality of service in downlink and uplink NOMA systems," *IEEE Trans. Wireless Commun.*, vol. 15, no. 11, pp. 7244–7257, November 2016.

[16] J. Cui, Z. Ding, and P. Fan, "A novel power allocation scheme under outage constraints in noma systems," *IEEE Signal Process. Lett.*, vol. 23, no. 9, pp. 1226–1230, September 2016.

[17] M. F. Kader, S. Y. Shin, and V. C. M. Leung, "Full-duplex non-orthogonal multiple access in cooperative relay sharing for 5g systems," *IEEE Trans. Veh. Technol.*, vol. 67, no. 7, pp. 5831–5840, July 2018.

[18] M. Salehi, H. Tabassum, and E. Hossain, "Meta Distribution of SIR in Large-Scale Uplink and Downlink NOMA Networks," *IEEE Trans. Commun.*, April 2019.

[19] S. P. Weber, J. G. Andrews, X. Yang, and G. De Veciana, "Transmission capacity of wireless ad hoc networks with successive interference cancellation," *IEEE Trans. Inf. Theory*, vol. 53, no. 8, pp. 2799–2814, 2007.

[20] S. R. Islam, N. Avazov, O. A. Dobre, and K.-S. Kwak, "Power-domain non-orthogonal multiple access (NOMA) in 5G systems: Potentials and challenges," *IEEE Commun. Surveys Tut.*, vol. 19, no. 2, pp. 721–742, 2017.

[21] M. Moltafet, P. Azmi, N. Mokari, M. R. Javan, and A. Mokdad, "Optimal and fair energy efficient resource allocation for energy harvesting-enabled-PD-NOMA-based HetNets," *IEEE Trans. Wireless Commun.*, vol. 17, no. 3, pp. 2054–2067, March 2018.

[22] C.-H. Liu and D.-C. Liang, "Heterogeneous networks with power-domain NOMA: coverage, throughput, and power allocation analysis," *IEEE Trans. Wireless Commun.*, vol. 17, no. 5, pp. 3524–3539, May 2018.

[23] M. Liu, J. Yang, and G. Gui, "Dsf-noma: Uav-assisted emergency communication technology in a heterogeneous internet of things," *IEEE Internet Things J.*, June 2019.

[24] Z. Ding, P. Fan, and H. V. Poor, "On the coexistence between full-duplex and noma," *IEEE Wireless Commun. Lett.*, Oct. 2018.

[25] A. Sahai, G. Patel, C. Dick, and A. Sabharwal, "On the impact of phase noise on active cancelation in wireless full-duplex," *IEEE Trans. Veh. Technol*, vol. 62, no. 9, pp. 4494–4510, 2013.

[26] L. Lei, E. Lagunas, S. Chatzinotas, and B. Ottersten, "Noma aided interference management for full-duplex self-backhauling hetnets," *IEEE Commun. Lett.*, vol. 22, no. 8, pp. 1696–1699, August 2018.

[27] V. Sharma, R. Sabatini, and S. Ramasamy, "Uavs assisted delay optimization in heterogeneous wireless networks," *IEEE Commun. Lett.*, vol. 20, no. 12, pp. 2526–2529, December 2016.

[28] L. Zhang, Q. Fan, and N. Ansari, "3-d drone-base-station placement with in-band full-duplex communications," *IEEE Commun. Lett.*, vol. 22, no. 9, pp. 1902–1905, September 2018.

[29] L. Zhang and N. Ansari, "On the number and 3-D placement of in-band full-duplex enabled drone-mounted base-stations," *IEEE Wireless Commun. Lett.*, vol. 8, no. 1, pp. 221–224, February 2018.

[30] T. Hou, Y. Liu, Z. Song, X. Sun, and Y. Chen, "Multiple antenna aided NOMA in UAV networks: A stochastic geometry approach," *IEEE Trans. Commun.*, 2018.

[31] N. Zhao, X. Pang, Z. Li, Y. Chen, F. Li, Z. Ding, and M.-S. Alouini, "Joint trajectory and precoding optimization for uav-assisted noma networks," *IEEE Trans. Commun.*, January 2019.

[32] W. Mei and R. Zhang, "Uplink cooperative NOMA for cellular-connected UAV," *IEEE J. Sel. Topics Signal Process.*, February 2019.

[33] A. A. Nasir, H. D. Tuan, T. Q. Duong, and H. V. Poor, "UAV-enabled communication using NOMA," *IEEE Trans. Commun.*, 2019.

[34] T. M. Nguyen, W. Ajib, and C. Assi, "A novel cooperative NOMA for designing UAV-assisted wireless backhaul networks," *IEEE J. Sel. Areas Commun.*, vol. 36, no. 11, pp. 2497–2507, November 2018.

[35] X. Yuan, Z. Feng, W. Xu, W. Ni, A. Zhang, Z. Wei, and R. P. Liu, "Capacity analysis of uav communications: Cases of random trajectories," *IEEE Trans. Veh. Technol.*, vol. 67, no. 8, pp. 7564–7576, Aug 2018.

[36] D. W. Matolak and R. Sun, "Air–ground channel characterization for unmanned aircraft systems part i: Methods, measurements, and models for over-water settings," *IEEE Trans. Veh. Technol*, vol. 66, no. 1, pp. 26–44, 2017.

[37] T. Z. H. Ernest, A. S. Madhukumar, R. P. Sirigina, and A. K. Krishna, "Outage Analysis and Finite SNR Diversity-Multiplexing Tradeoff of Hybrid-Duplex Systems for Aeronautical Communications," *IEEE Trans. Wireless Commun.*, April 2019.

[38] ——, "Hybrid-Duplex Communications for Multi-UAV Networks: An Outage Probability Analysis," *IEEE Commun. Lett.*, 2019.

[39] T. Hou, Y. Liu, Z. Song, X. Sun, and Y. Chen, "Exploiting NOMA for UAV Communications in Large-Scale Cellular Networks," *IEEE Trans. Commun.*, 2019.

[40] N. Zlatanov, E. Sippel, V. Jamali, and R. Schober, "Capacity of the gaussian two-hop full-duplex relay channel with residual self-interference," *IEEE Trans. Commun.*, vol. 65, no. 3, pp. 1005–1021, 2017.

[41] Y. Wang, Q. Cui, M. Haenggi, and Z. Tan, "On the sir meta distribution for poisson networks with interference cancellation," *IEEE Wireless Commun. Lett*, 2017.

[42] M. F. Kader and S. Y. Shin, "Coordinated direct and relay transmission using uplink NOMA," *IEEE Wireless Commun. Lett.*, vol. 7, no. 3, pp. 400–403, June 2018.

[43] G. Im and J. H. Lee, "Outage probability for cooperative noma systems with imperfect sic in cognitive radio networks," *IEEE Commun. Lett.*, vol. 23, no. 4, pp. 692–695, April 2019.

[44] K. A. Hamdi, "A useful lemma for capacity analysis of fading interference channels," *IEEE Trans. Commun.*, vol. 58, no. 2, pp. 411–416, February 2010.

[45] M. O. Hasna, M.-S. Alouini, A. Bastami, and E. S. Ebbini, "Performance Analysis of Cellular Mobile Systems with Successive Co-Channel Interference Cancellation," *IEEE Trans. Wireless Commun.*, vol. 2, no. 1, pp. 29–40, January 2003.

[46] Y. Sun, D. W. K. Ng, J. Zhu, and R. Schober, "Robust and secure resource allocation for full-duplex MISO multicarrier NOMA systems," *IEEE Trans. Commun.*, vol. 66, no. 9, pp. 4119–4137, September 2018.

[47] 3GPP TR36.777, "Study on Enhanced LTE Support for Aerial Vehicles," Tech. Rep., 2017.

[48] Y.-S. Choi and H. Shirani-Mehr, "Simultaneous transmission and reception: Algorithm, design and system level performance," *IEEE Trans. Wireless Commun.*, vol. 12, no. 12, pp. 5992–6010, 2013.